Robotica (2017) volume 35, pp. 876–891. © Cambridge University Press 2015
doi:10.1017/S0263574715000867

Horizontal path following for underactuated AUV based on dynamic circle guidance

Huang Xinjing, Li Yibo*, Du Fei and Jin Shijiu

State Key Laboratory of Precision Measurement Technology and Instrument, Tianjin University, Tianjin, China
E-mails: huangxinjing@tju.edu.cn, dukemyy@tju.edu.cn, shjjin@tju.edu.cn

(Accepted September 29, 2015. First published online: November 2, 2015)

SUMMARY
A 2D path following control method for Autonomous Underwater Vehicles (AUVs) based on dynamic circle heading modification (DCHM) is presented. The method makes a dynamic auxiliary circle, whose radius depends on the cross-track error e, to intersect the desired path to get a new expected path point, and then determines a modified expected heading for the AUV. The guidance function is achieved by a direct mapping between e and the heading modification value Ψ_m. Several cases are tested in order to demonstrate the performance of the guidance and control method based on DCHMs for a real AUV. Results show that methods using a convex mapping function between e and Ψ_m based on our new idea can easily achieve a better convergence of path following, and reduce the error between the actual and desired heading angles. We can also customize a discretionary mapping between e and Ψ_m to get better path following performance.

KEYWORDS: Underactuated AUV; Path following; Control; Line-of-sight guidance; Dynamic circle guidance.

1. Introduction

AUVs are often used to survey underwater topography and seabed geology in specified unknown waters using various subaqueous measurement systems, such as side-scan sonar, shallow profile sonar, and multi-beam sonar.[1–4] These sonar measurement devices usually scan a limited geometrical bandwidth, which is about 300 m wide in the direction perpendicular to the AUV's forward direction and is related to the height of the AUV to the seabed.[5–7] The AUV needs to scan back and forth in a horizontal plane for multiple measurements. As shown in Fig. 1, a lawn-mower pattern is common in sea floor surveying applications. It is a combination of many straight line paths, of which the longer line is a scanning path ranging from several hundred meters to tens of kilometers and the shorter line is a turning around path generally ranging from 150–200 m. Analyses of those sonar devices' data need consideration of AUV's attitude and deviation from the straight path at every sample point. The more stable the attitude is and the smaller the deviation is, the more accurate the measurement results are. It is necessary for the AUV to travel precisely along a specified path in a horizontal plane, which is actually a 2D path following issue.

Path following usually involves the separate construction of the geometric path and the dynamic assignment, and emphasizes spatial localization as the primary task objective, but considers the dynamic aspect to be of secondary importance.[8] Pioneering work on the type of path following scheme under consideration can be found in ref. [9], where the author considers path following for wheeled mobile robots. There is plenty of literature[10–18] on path following for aerial vehicles, under-actuated ships, and under-actuated and fully-actuated AUV. Generally, path following control systems for these autonomous vehicles are functionally divided into three subsystems that must be implemented on board: guidance, navigation, and control.[19] The Guidance subsystem computes the reference (desired) position, velocity, and acceleration of the vehicle to be used by the control system; the Navigation subsystem provides the vehicle's position, course, and velocity; and the Control

* Corresponding author. E-mail: 1207571368@qq.com

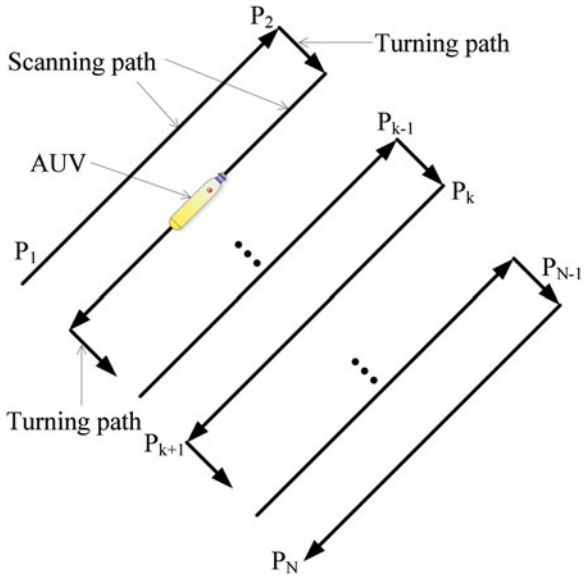

Fig. 1. Desired paths that AUV is to follow.

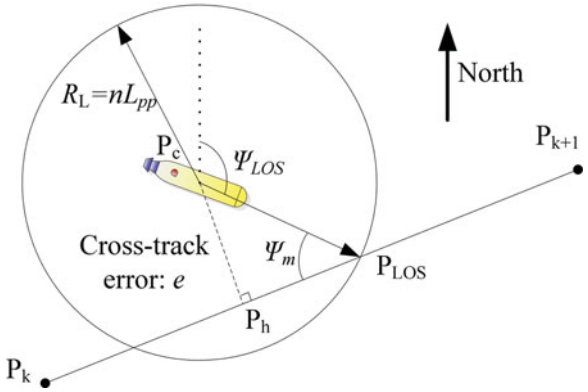

Fig. 2. Illustration of Line-Of-Sight guidance.

subsystem determines the necessary control forces and moments to be provided by the vehicle in order to satisfy a given control objective. The desired control objective is usually in conjunction with, and must adapt to, the guidance system. With a reasonable guidance method, good path following performance can be achieved using rather simple or common heading control methods.

Line of sight (LOS) guidance is the most widely used guidance strategy today among various guidance methods.[20–22] In fact, almost all guidance laws in use today have some form of LOS guidance because of its simplicity and ease of implementation. The claim is that if a vehicle is able to keep its heading aligned with the so-called LOS angle Ψ_{LOS}, as shown in Fig. 2, convergence to desired position is also achieved. The LOS vector can be defined as the vector from the vessel's current position $\mathrm{P}_c(x_c, y_c)$ to the intersecting point on the path $\mathrm{P}_{\mathrm{LOS}}(x_{LOS}, y_{LOS})$, with a distance of n times vehicle's length L_{pp} ahead of the vessel. Thus, the desired heading angle Ψ_{LOS} can be computed as formulae (1)–(3). However, because the length of the LOS vector R_L in the basic LOS method is constant, the convergence performance of the basic LOS is usually not adequate enough when a better path following performance is necessary.

$$\psi_{LOS} = a\tan2(y_{LOS} - y, x_{LOS} - x), \tag{1}$$

where the LOS coordinates (x_{LOS}, y_{LOS}) are given by

$$(y_{LOS} - y)^2 + (x_{LOS} - x)^2 = (nL_{pp})^2, \tag{2}$$

https://doi.org/10.1017/S0263574715000867 Published online by Cambridge University Press

Fig. 3. Tianjin University's AUV equipped with a vectored thruster.

$$\left(\frac{y_{LOS}-y_k}{x_{LOS}-x_k}\right)=\left(\frac{y_{LOS}-y_{k+1}}{x_{LOS}-x_{k+1}}\right)=\text{constant}. \tag{3}$$

The initial inspiration for the work reported here can be traced back to ref. [24] where the n of basic LOS is constant, which can be called LOS guidance based on *Constant Circle Heading Modification* (CCHM); and ref. [19], where the n of improved LOS is time-varying. The latter can guarantee a smaller cross-track error and a shorter setting distance. Other LOS methods such as[19] first design a method of using e to calculate the temporary desired way point for determination of the LOS vector, and then to calculate the Ψ_{LOS}. However, they never consider a direct mapping function between the cross-track error e and the heading angle modification Ψ_m. Their path following performances need verification, especially when suffering a shocking disturbance (the beginning and turning path of the path following are similar to sudden shocks). We claim this idea can bring more certain and predictable convergence characteristics of path following.

This paper therefore introduces a practical guidance and control system, based on DCHM, with a direct mapping function between the cross-track error e and the heading angle modification Ψ_m, used to improve the convergence of the traditional LOS algorithm when applied to the AUV's path following. Several cases are tested in order to demonstrate the performance of the guidance and control design, based on DCHM for a real AUV produced by Tianjin University as shown in Fig. 3.[23] The AUV is about $\varphi 0.8$ m $\times$ $L8$ m, and is designed to dive 3000 m deep to survey the seabed. The whole system will be implemented and evaluated through tests that can be performed in lakes and then in seas.

The DCHM method belongs to the LOS guidance group, which can diminish the 3 DOF position and heading control objective of a thruster and rudder powered AUV carrying out horizontal path following[24] to a 2 DOF (heading and surge) control objective.

2. Guidance Based on DCHM

Table I describes all symbols in this paper. The lawn-mower pattern is defined by the corner points $\{P_1, P_2, \ldots, P_k, P_{k+1}, \ldots, P_N\}$. When the AUV moves along the current sub-path $\overrightarrow{P_{k-1}P_k}$, the next sub-path $\overrightarrow{P_kP_{k+1}}$ can be switched by selecting the way point (x_{k+1}, y_{k+1}) on a basis of whether the AUV lies within a circle of acceptance with radius R_0 around the way point (x_k, y_k). R_0 has a great influence on AUV's path following performance near the path corners. Thus every sub-path can be treated the same when it is followed by AUV via LOS method.

As shown in Fig. 4, the New DCHM guidance method uses a direct mapping function between the cross-track error e and the heading angle modification Ψ_m, while old LOS methods, such as CCHM and old DCHM (see Table II) from refs.[24] and [19] use two more temporary intermediate variables instead. The cross-track error e, denotes the distance between the AUV's current position $P_c(x_c, y_c)$ and its orthogonal projection $P_h(x_h, y_h)$ on the current sub-path, as in Eq. (4). R_L is a function of e. For example, CCHM and old DCHM try Eqs. (5) and (6), respectively. However, we believe knowledge

https://doi.org/10.1017/S0263574715000867 Published online by Cambridge University Press

Table I. Description of all symbols in this paper.

Name	Description
Ψ_{LOS}	LOS heading angle.
R_L	Radius of dynamic circle.
L_{pp}	Length of vehicle.
e	Path following error.
Ψ, Ψ_c, Ψ_d	Any, current, desired heading angle relative to North. Ψ_d=Ψ_{LOS}.
Ψ_m	See Fig. 2.
e_{max}	If $e > e_{max}$, $\Psi_m = 90^\circ$.
x,y	Position in WE and NS directions relative to any fixed point.
$\boldsymbol{\eta}$, $\boldsymbol{\eta}_c$	(x,y, Ψ) and current $\boldsymbol{\eta}$.
u,v	Surge and sway speed.
r	Rate of heading angle.
$\boldsymbol{\nu}$, $\boldsymbol{\nu}_c$	(u,v,r) and current ν.
x_l	See Fig. 6.
$\mathbf{D}$,$\mathbf{M}$,τ	See formulas (17), (18), (19).
δ,δ_c,δ_d	Any,current, desired rudder angle.
Other symbols in (17)–(20).	They are elements of inertia matrix of rigid-body and its added mass. See ref. [25], Chapter 3.1.

Table II. Different methods to be tested.

Name	Method	Conform to formulae (9), (10)?
CCHM	Formula (11)	No
Old DCHM	Formula (12)	Yes
New DCHM1	Formula (13), $n = 0.6$	Yes
New DCHM2	Formula (13), $n = 1$	No
New DCHM3	Formula (13), $n = 2$	No
New DCHM4	Curve 6 in Fig. 5, improved new DCHM1.	Yes, and improved.

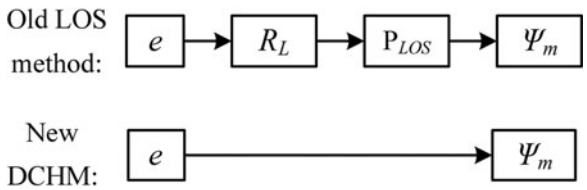

Fig. 4. New DCHM's feature.

of R_L is not required. The relationship between e and R_L is shown in Eq. (7).

$$e = \frac{|Ax_c + By_c + C|}{\sqrt{A^2 + B^2}}, \overrightarrow{P_{k-1}P_k} : Ax + By + C = 0 \tag{4}$$

$$R_L = nL_{pp} \tag{5}$$

$$R_L = e + L_{pp} \tag{6}$$

$$\sin \psi_m = \frac{e}{R_L}. \tag{7}$$

In our new approach, a more concise LOS guidance is shown in Eqs. (8)–(10). e_{max} is a demarcation value of e. If $e \geq e_{max}$, $\Psi_m = 90^\circ$, and the AUV will be controlled to move forward perpendicular to the current sub-path. Thus, e will decrease most rapidly. If $e < e_{max}$, the AUV will be controlled to move in the direction $\Psi_m = f(e)$. $f(e)$, as shown in Eqs. (9) and (10), must be a monotonically increasing and convex function, because when a large e appears, a large heading modification can be exerted rapidly and continuously upon the AUV. Conversely, when e becomes small, the AUV can

https://doi.org/10.1017/S0263574715000867 Published online by Cambridge University Press

also reduce its heading modification in time.

$$\psi_m = \begin{cases} f(e), \forall e \in [0, e_{\max}) \cdots (a) \\ 90^\circ, \quad \forall e \in [e_{\max}, +\infty) \cdots\cdots\cdots\cdots (b) \end{cases} \tag{8}$$

$$\frac{df(e)}{de} > 0, \ \forall e \in [0, e_{\max}) \tag{9}$$

$$\frac{d^2 f(e)}{de^2} < 0, \ \forall e \in [0, e_{\max}). \tag{10}$$

In Fig. 4, the value for R_L is usually unknown, and chosen after many trials. Even if a function map of R_L and e (as well as any other parameters) has been determined, Ψ_m will still have to be computed in order to navigate AUV. This proves the excrescence of R_L. We propose that a direct mapping between Ψ_m and e should be used. We therefore introduce Eqs. (9) and (10), the basic principles of the function map of Ψ_m and e. All equations in accordance with Eqs. (9) and (10) can achieve path following for the AUV.

One may intuitively think that it would be functional enough for R_L and e to have a negative correlation (that is, R_L decreases as e increases), as this will bring about a big heading modification Ψ_m if e is rather big. However, this method does not directly calculate the Ψ_m using e. We select several different methods using different mappings from e to Ψ_m, to verify the effectiveness of our new approach. As shown in Table II, some of the methods are based on the direct mapping between e and Ψ_m, such as new DCHM1–4; while others are not, such as CCHM and Old DCHM coming from papers [24] and [19] respectively. In addition, New DCHM4 uses a custom mapping from e to Ψ_m to eliminate New DCHM1's slight overshoot appearing in following case study:

$$\psi_m = \begin{cases} \operatorname{asin}\left(\frac{e}{nL_{pp}}\right), \forall e \in [0, e_{\max}) \\ 90^\circ, \forall e \in [e_{\max}, +\infty) \end{cases} \tag{11}$$

$$\psi_m = \operatorname{asin}(\frac{e}{R_L}) = \operatorname{asin}(\frac{e}{e + L_{pp}}), \forall e \in [0, +\infty) \tag{12}$$

$$\psi_m = \begin{cases} 90^\circ \left(\frac{e}{e_{\max}}\right)^n, n > 0, \forall e \in [0, e_{\max}) \\ 90^\circ, \forall e \in [e_{\max}, +\infty) \end{cases}. \tag{13}$$

The mapping relationships between e and Ψ_m in the above guidance methods are shown in Fig. 5. CCHM and new DCHM3 are concave. DCHM2 is linear. Old DCHM, new DCHM1, and new DCHM4 are convex. It is noteworthy to observe that when e is large, Ψ_m of Old DCHM increases rather slowly while Ψ_m of New DCHM4 increases quite rapidly. We can customize a discretionary mapping between e and Ψ_m without intentionally selecting a mapping function of R_L and e in advance—whose guidance performance is indistinct and is difficult to control.

3. Implementation of DCHM in a Real the AUV

3.1. Three DOFs horizontal kinematics of the AUV

Here, we use two reference frames:

3.1.1. North-east-down frame (NED). This is a reference frame defined relative to the reference ellipsoid of the earth as described by WGS 84. The frame has its origin at some point on the earth's surface where the x- and y-axes spans a tangent plane to the earth's surface, while the z-axis points down into the earth. The x-axis points towards true north, hence the y-axis points towards east.

3.1.2. BODY fixed frame. A reference frame which is fixed at a point located on the vessel under consideration. This is by all means not an inertial reference frame. The axes are often chosen along the principal axes of inertia, hence the x-axis is longitudinal (from stern to bow) and the y-axis transversal

https://doi.org/10.1017/S0263574715000867 Published online by Cambridge University Press

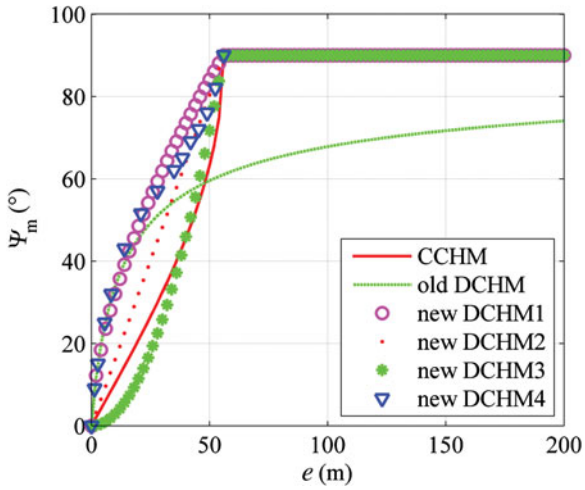

Fig. 5. Mappings between e and Ψ_m of different methods.

(from port to starboard). The z-axis points downwards, orthogonal to the plane spanned by the x- and y-axes in accordance with the convention set by the NED frame.

Since we only consider the three horizontal DOFs, the kinematic relationship between the NED frame and the BODY frame can be simplified since the roll and pitch angles are assumed small. In fact, the relationship is derived in Chapter 3.1, Page 22 of ref. [24] and is given by

$$\dot{\boldsymbol{\eta}} = \mathbf{R}(\psi)\boldsymbol{\nu}, \tag{14}$$

where

$$\mathbf{R}(\psi) = \mathbf{R}_{z,\psi} = \begin{bmatrix} \cos(\psi) & -\sin(\psi) & 0 \\ \sin(\psi) & \cos(\psi) & 0 \\ 0 & 0 & 1 \end{bmatrix} \tag{15}$$

is the rotation matrix transforming motion from the non-inertial, vessel-fixed BODY frame to the assumed-to-be-inertial, earth-fixed NED frame. $\boldsymbol{R}(\Psi)$ represents a rotation about the z-axis of the NED frame by an angle Ψ. $\boldsymbol{\eta} = [x,y,\Psi]^T$ represents the earth-fixed position (x,y) and heading Ψ(NED), while $\nu = [u,v,r]^T$ represents the corresponding vessel-fixed surge, sway, and yaw velocities (BODY).

For the AUV equipped with a vectored thruster whose rudder angle is very small (not exceeding $\pm 20^\circ$), its horizontal and vertical motions can be decoupled. It is therefore reasonable to simplify the AUV's mathematical model into a 3 DOF (surge–sway–yaw) linear manoeuvring model as Eqs. (16)–(19).[25] Here, $\mathbf{M}$ includes the added mass system inertia matrix $\mathbf{M}_A$ and the rigid-body system inertia matrix $\mathbf{M}_{RB}$, and the Coriolis-centripetal matrix is negligible for low-speed applications of AUV. Figure 6 illustrates the push force and moment in Eq. (19).

$$\mathbf{M}\dot{\boldsymbol{\nu}} + \mathbf{D}\boldsymbol{\nu} = \boldsymbol{\tau}, \tag{16}$$

where

$$\mathbf{D} = \begin{pmatrix} -X_u & 0 & 0 \\ 0 & -Y_v & -Y_r \\ 0 & -N_v & -N_r \end{pmatrix} = \begin{pmatrix} 198.12 & 0 & 0 \\ 0 & 1442.33 & -271.09 \\ 0 & -310.72 & 6964.59 \end{pmatrix}, \tag{17}$$

https://doi.org/10.1017/S0263574715000867 Published online by Cambridge University Press

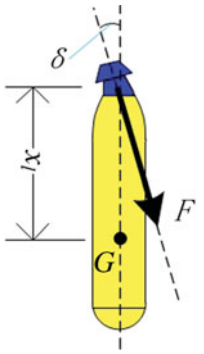

Fig. 6. Illustration for push force and moment.

$$\mathbf{M} = \mathbf{M}_A + \mathbf{M}_{RB} = \begin{pmatrix} m - X_{\dot{u}} & 0 & 0 \\ 0 & m - Y_{\dot{u}} & mx_g - Y_{\dot{r}} \\ 0 & mx_g - Y_{\dot{r}} & I_z - N_{\dot{r}} \end{pmatrix} = \begin{pmatrix} 3316.36 & 0 & 0 \\ 0 & 3633.80 & 534.53 \\ 0 & 534.53 & 41337.24 \end{pmatrix}, \tag{18}$$

$$\boldsymbol{\tau} = [F\cos(\delta) \quad F\sin(\delta) \quad F\sin(\delta)x_l]^T \approx [F \quad F\delta \quad 4.5F\delta]^T. \tag{19}$$

3.2. Steering characteristics and control of AUV

We conducted an open-loop simulation of the AUV's movement, using the matrix Eqs. (16)–(19), according to ref. [25] under the conditions that the AUV is given a fixed rudder angle δ and push force F without any feedback control. We listed different sway velocities v and rudder angles δ. We find that δ has a linear impact on AUV's sway velocity v when F is constant and $\delta[-20^\circ, +20^\circ]$, and v eventually tends to be constant when a fixed rudder angle is given.

Finally, from Eq. (16), we can get Eq. (20), taking into account the characteristics of the AUV's actual response. The AUV's steering kinematics is thus computed to be Eq. (21).

$$\begin{cases} -Y_{\dot{r}}\dot{v} + (I_z - N_{\dot{r}})\dot{r} - N_v v - N_r r = 4.5F\delta \\ \dot{v} = 0|_{t\to+\infty} \\ v = k\delta|_{t\to+\infty},\ k = 3.1375\,\mathrm{m/(s\cdot rad)} \end{cases} \tag{20}$$

$$(I_z - N_{\dot{r}})\dot{r} - N_r r = (Fx_l + N_v k)\delta. \tag{21}$$

Considering Eqs. (17), (18), (22), we can finally get Eq. (23).

$$\dot{\psi} = r \tag{22}$$

$$\frac{\psi}{\delta}(s) = \frac{K}{s(1+Ts)}, \tag{23}$$

where

$$K = \left.\frac{Fx_l + N_v k}{-N_r}\right|_{F=400\mathrm{N}} = 0.3755\mathrm{s}^{-1}, \tag{24}$$

$$T = \frac{I_z - N_r}{-N_r} = 9.1232\mathrm{s}. \tag{25}$$

We must also carefully consider that the rudder angle changes with a time-delay proportional to the difference between the desired and actual steering rudder angle. This is because the rudder motor's

https://doi.org/10.1017/S0263574715000867 Published online by Cambridge University Press

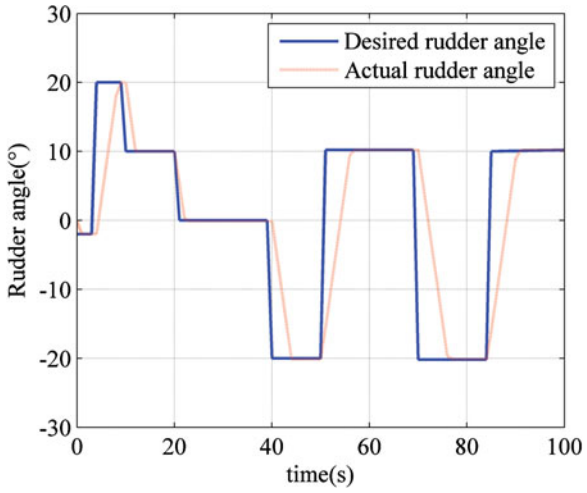

Fig. 7. Performance of the horizontal rudder.

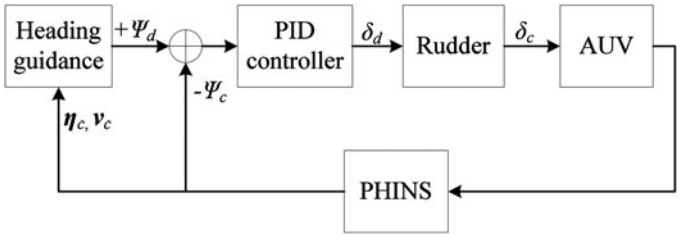

Fig. 8. Steering control loop of the AUV.

rotation is uniform and can take considerable time if the difference between the desired and current angles is large. Equation (26) describes the mathematical model of the AUV's horizontal rudder. Figure 7 shows the horizontal rudder's performance.

$$\delta_c(t) = \begin{cases} \delta_{c\max}, \delta_c(t) > \delta_{c\max} \\ \frac{\delta_c(t)-\delta_d(t)}{|\delta_c(t)-\delta_d(t)|} at, |\delta_c(t)| \le \delta_{c\max}, \\ -\delta_{c\max}, \delta_c(t) < -\delta_{c\max} \end{cases} \tag{26}$$

where $a = 6^\circ/\text{s} = 0.1047$ rad/s is the constant angular velocity of the AUV's rudder, and δ_c, and δ_d denote desired and actual current (or output and input) rudder angles respectively.

As shown in Fig. 8, the heading guidance calculates a desired heading angle $\Psi_d = \Psi_{LOS}$ using the AUV's current $\boldsymbol{\eta}_c$ and $\boldsymbol{\nu}_c$. The PID controller as described by Eq. (27) calculates a desired rudder angle δ_d using Ψ_d and the AUV's current Ψ_c. The rudder then rotates an actual angle with a time-delay as seen in Eq. (26) to drive the AUV to adjust its heading. The AUV's current η_c and ν_c are measured by PHINS (Photonic Inertial Navigation System) in a real AUV. The PID controller's responses to different step signals of desired heading angles are shown in Fig. 9.

$$\delta_d(s) = -K_p\left(1 + T_d s + \frac{1}{T_i s}\right)\tilde{\psi}(s), \tag{27}$$

where

$$\tilde{\psi} = \psi_d - \psi_c, \tag{28}$$

https://doi.org/10.1017/S0263574715000867 Published online by Cambridge University Press

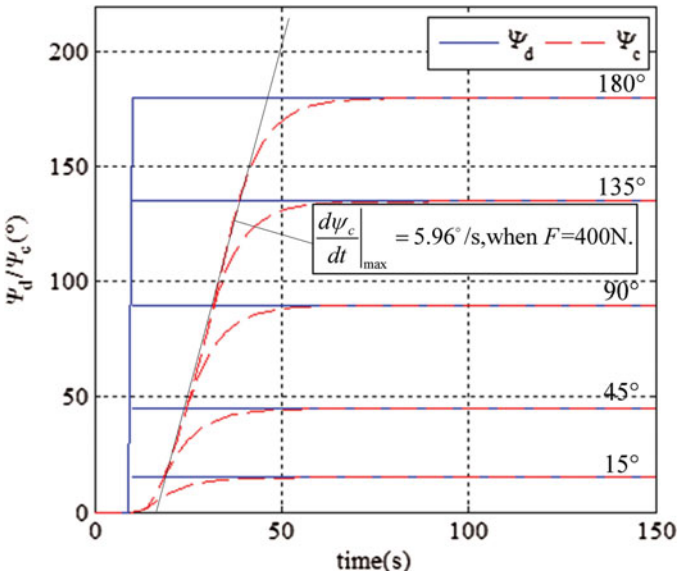

Fig. 9. PID controller's performance.

$$K_p = 1.223,$$
$$T_d = 9.708,$$
$$T_i = +\infty.$$

The New DCHMs' guidance with a PID controller is globally stable, because it belongs to LOS guidance groups. This is a concrete practical case of LOS method. Theorem 5.1 in ref. [24] has proven this in detail: "The LOS controller becomes Uniformly Globally Asymptotically Stable by choosing the control and disturbance adaptation law as Eqs. (5.21) and (5.22), respectively". The LOS controller derived in Chapter 5 of ref. [24] can be used by fully actuated or underactuated vessels with any LOS guidance system to perform path following.

4. Simulation Results

In this section, case studies will be presented to compare the path following trajectories based on different methods in Table II. The AUV's model used in the simulation is presented in Fig. 2 and Section 3.1. The desired path consists of eight way points:

$$\mathrm{Wpt}_1(0, 0)\mathrm{m},\ \mathrm{Wpt}_2(20, 5)\mathrm{m},$$
$$\mathrm{Wpt}_3(30, 50)\mathrm{m},\ \mathrm{Wpt}_4(15, 60)\mathrm{m},$$
$$\mathrm{Wpt}_5(15, 80)\mathrm{m},\ \mathrm{Wpt}_6(30, 90)\mathrm{m},$$
$$\mathrm{Wpt}_7(20135)\mathrm{m},\ \mathrm{Wpt}_8(0140)\mathrm{m}.$$

The AUV's initial states for the trajectory are

$$\boldsymbol{\eta}_0 = (x_0, y_0, \Psi_0) = (200\,\mathrm{m},\ -150\,\mathrm{m},\ -90^\circ),$$
$$\mathbf{v}_0 = (u_0, v_0, r_0) = (0\,\mathrm{m/s}, 0\,\mathrm{m/s}, 0^\circ/\mathrm{s}).$$

The desired speed is kept constant with a value of 2.01 m/s when the push force F is 400 N, as F is almost independent of the rudder angle due to its small range from -20° to $+20^\circ$. The procedure to calculate the Ψ_{LOS}, namely Ψ_d, is shown in Fig. 10. Figure 11 shows an xy-plot of the AUV's

https://doi.org/10.1017/S0263574715000867 Published online by Cambridge University Press

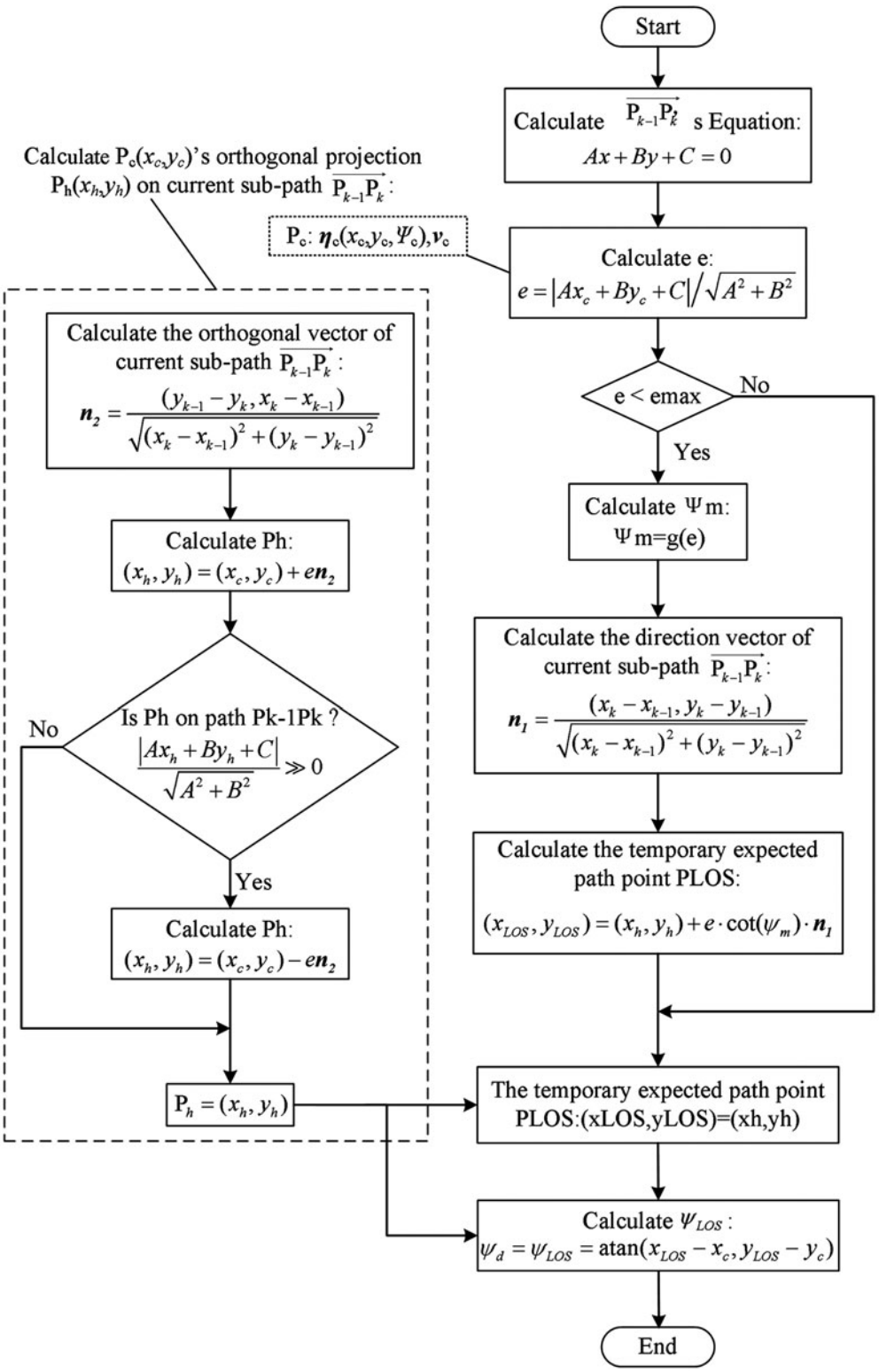

Fig. 10. Procedure for calculating Ψ_{LOS}.

position using the six methods together with the desired geometrical path consisting of straight line segments with no ocean currents. Figure 11 (a) presents a general view. Figure 11 (b) is a detailed view of area A containing the starting process. Figure 11 (c) is a detailed view of area B containing the turning back process. Figure 12 shows an *xy*-plot of the simulated actual and desired geometrical paths using different methods under a 1 m/s ocean current. An *xy*-plot of the simulated actual and

https://doi.org/10.1017/S0263574715000867 Published online by Cambridge University Press

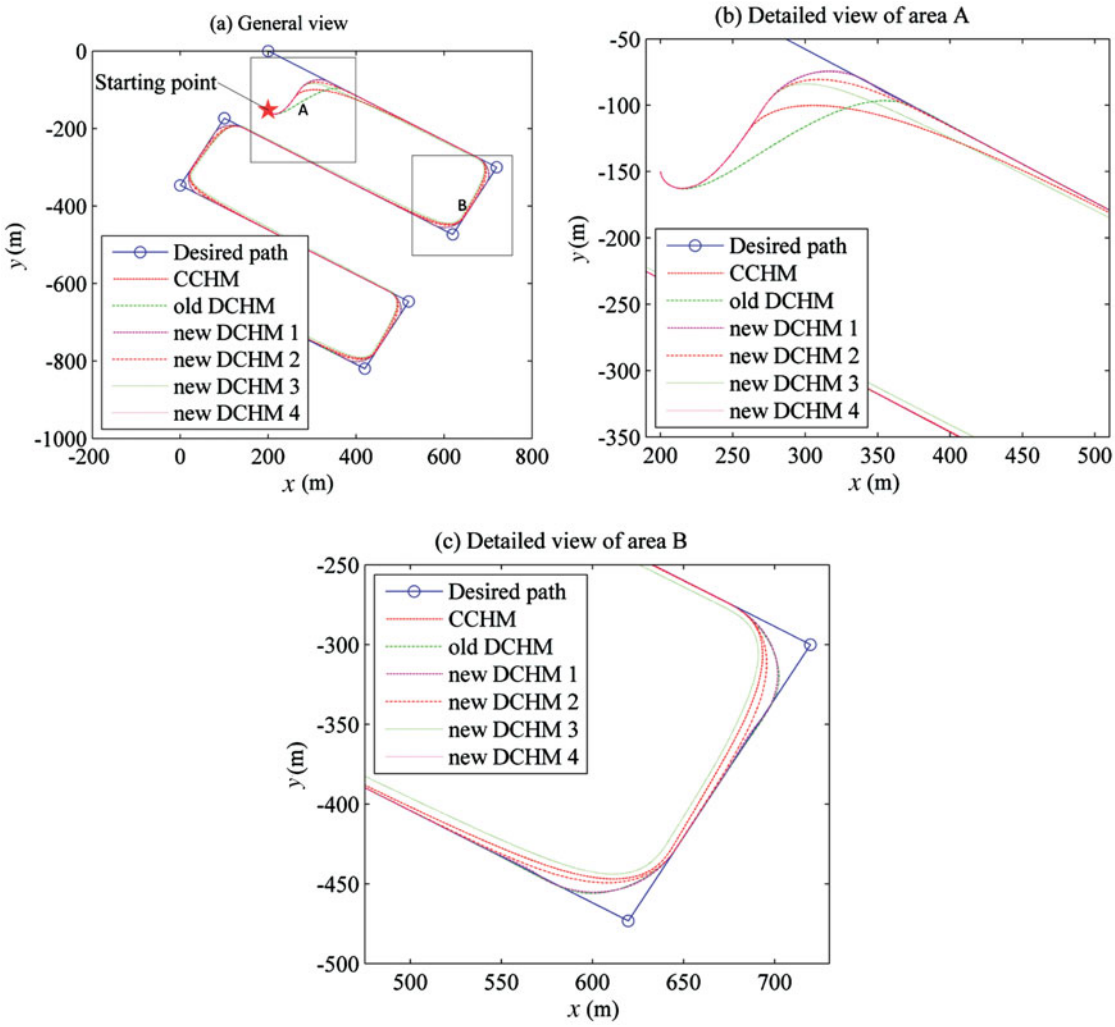

Fig. 11. *xy*-plot of the simulated and desired paths using different methods in Table II.

desired geometrical paths, using new DCHM4 under ocean currents from 0 to 1.8 m/s, is shown in Fig. 13.

4.1. Path following performance with no ocean currents

As shown in Fig. 11, although all the above mentioned methods can complete the AUV's path following, they converge to the desired path at different speeds. The methods using a concave mapping from e to Ψ_m suffer a very long setting distance once the AUV deviates from the desired path, or needs to switch to the next sub-path. All methods using a convex mapping from e to Ψ_m, except Old DCHM, achieve very short setting distances when the AUV returns to the desired path even with very bad initial conditions as shown in Fig. 11 (b). Additionally, they can complete path switching with very short distances as shown in Fig. 11 (c). Using these methods, the AUV can closely and enduringly follow the desired path, with an even greater effective path following mileage. This can guarantee minimal energy consumption. The Old DCHM method cannot drive the AUV to return to the desired path from a large deviation as fast as the New DCHM1, New DCHM4, and even New DCHM 2 (linear), because Ψ_m of old DCHM increases quite slowly when e is big.

4.2. Path following performance under ocean currents

From Fig. 12, we can find that the 1 m/s ocean current causes different path following errors using different methods. Errors of convex mapping methods such as those of Old DCHM, new DCHM1,

https://doi.org/10.1017/S0263574715000867 Published online by Cambridge University Press

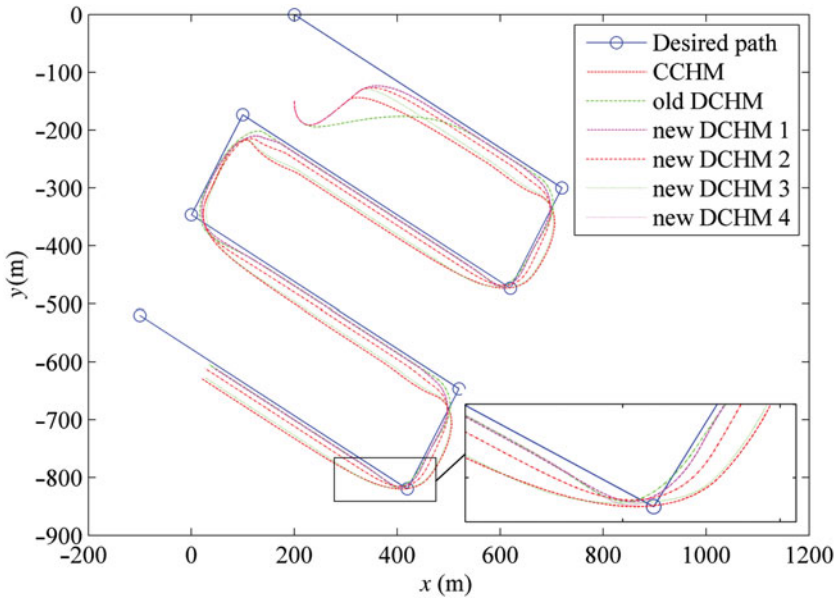

Fig. 12. *xy*-plot of the simulated and desired geometrical paths using different methods under a 1 m/s ocean current (in –*y* direction).

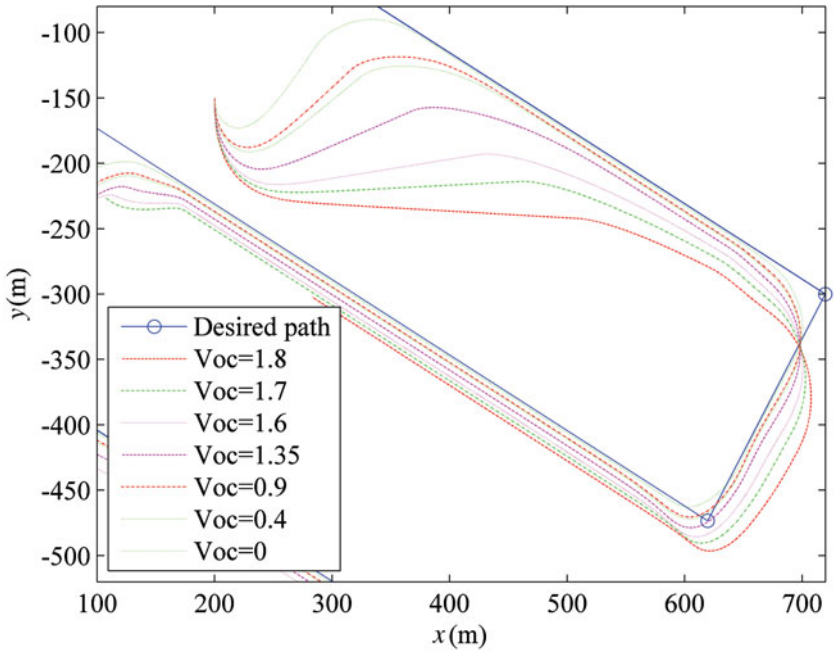

Fig. 13. *xy*-plot of the simulated and desired geometrical paths using new DCHM4 under different ocean currents from 0–1.8 m/s (in –*y* direction).

and DCHM4, are much smaller than those of concave and linear mapping methods, such as CCHM, new DCHM2, and DCHM3.

From Fig. 13, we can deduce that under 0–1.8 m/s ocean currents, the path following error of the proposed DCHM4 method increases with the increase in the ocean current velocity. Meanwhile, the error can be kept constant as the AUV moves along longer paths. The bias can be explained as such: In order to overcome ocean currents, the AUV's heading angle cannot be parallel to the desired path, and hence will cause non-zero values of Ψ_m, which is mapped onto different values of biases.

This kind of bias can be easily removed when we process sonar images. However, we still have one method to compensate the bias caused by ocean currents: when this bias is sensed by the AUV

https://doi.org/10.1017/S0263574715000867 Published online by Cambridge University Press

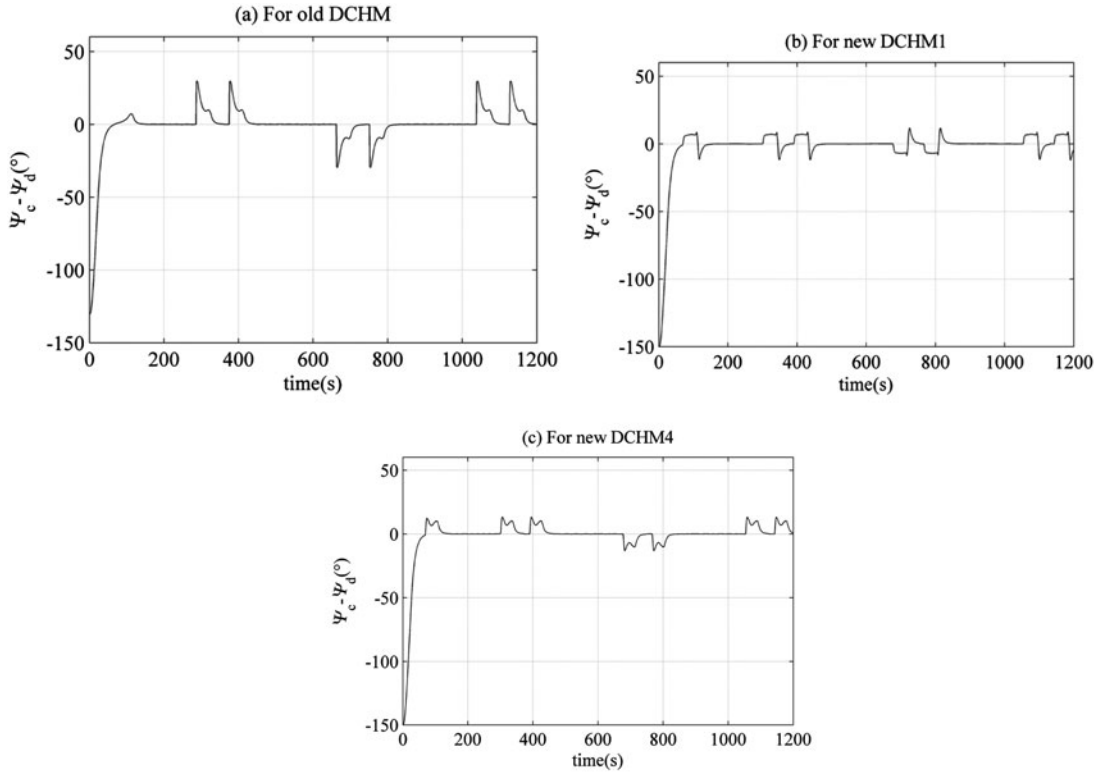

Fig. 14. plot of the error Ψ_c–Ψ_d for old DCHM, new DCHM1, and new DCHM4.

for a given time period, it can change the Ψ_m and reduce the path following error to an expected small value using historic integral error, and then recover the previous heading modification Ψ_{m1}. As such, there will be small oscillations around the desired path and the rudder will be able to keep still, which can guarantee the normal performance of the scanning sonar system.

In addition, when the velocity of the ocean current v_{oc} is very large, the proposed method will fail. For example, when $v_{oc} > 2.01$ m/s, non-convergence of the AUV's path following often occurs. This is because the max velocity of the AUV with a push force $F = 400$ N is 2.01 m/s, and therefore the AUV will completely lose control when $v_{oc} > 2.01$ m/s.

4.3. Heading control performance

Figure 14 (a)–(c) presents the error/difference between the actual and desired heading angle using different DCHMs conforming to Eqs. (7)–(10). The new DCHMs can minimize the error between the actual and desired heading angle and can reduce the time during which such error exists. Methods shown here are all convex, but only the new DCHM1 and 4 are designed based on our new idea of using a direct mapping function between the e and Ψ_m. Particularly, the New DCHM4 uses a custom mapping from e to Ψ_m. The maximal heading errors are 30°, 13°, 13°, for the Old DCHM, New DCHM1, and New DCHM4, respectively. The times during which the errors exist are 60 s, 60 s, 50 s, for the Old DCHM, New DCHM1, and New DCHM4, respectively.

4.4. Performance measures

Table III lists the results of performance measures for different methods with no ocean currents as well as under a 1 m/s ocean current. To follow a given path, the total actual travel distance spent by New DCHM4 is the shortest among those spent by all methods tested. New DCHM1, 2, and 4 spend shorter total distances than all other methods. Ocean currents can lengthen total distances of all methods, but does not change the performance order of total distances.

The average energy consumption of a lawn-mower pattern path is almost independent of ocean currents, and different methods consume almost the same amount of energy, since the energy

https://doi.org/10.1017/S0263574715000867 Published online by Cambridge University Press

Table III. Performance measures of different methods with no ocean currents and under a 1 m/s ocean current[1].

Methods	Total distance (m)		Energy cons.[b] (kW h)		Mean error[c] (m)		Max Error[d] (m)		Non-qualified distance[e](m)	
CCHM	2044.6	2154.2	170.9	171.0	0.8	37.7	15.4	39.0	1020.1	682.3
Old DCHM	2046.9	2144.0	171.2	171.2	<0.2	7.0	5.2	7.5	486.3	703.5
New DCHM1	2020.8	2104.0	172.4	172.5	<0.2	7.3	6.1	8.0	460.8	554.8
New DCHM2	2026.4	2119.7	171.1	171.1	0.32	15.9	12.5	17.0	466.6	544.6
New DCHM3	2032.0	2130.0	171.0	171.1	6.3	32.5	18.0	34.0	1282.9	670.1
New DCHM4	2018.0	2102.4	171.1	171.2	<0.2	6.6	5.0	7.1	458.0	513.7

[a]For each performance measure: left – with no ocean current; right – under ocean current 1 m/s.
[b]Energy consumption, calculation method: $E = P1*T1+P2*T2$, P1-power of push motor, P1 = 500 W; T1-total time during which push propeller rotates, T1 = 1200 s; P2-power of rudder motor, P2 = 30 W; T2-total time during which push rudder is active.
[c,d]the average and maximum error of path following respectively, without considering starting part of actual path in area A in Fig. 11 (a).
[e]Qualified distance, the total length of actual move path where tracking error is continuously varying. This kind of error cannot be removed easily when we process sonar images. Only long paths are considered since the sonar images along the short paths will be discarded.

consumption by the propeller is almost constant, and accounts for more than 90% of the total energy.

Mean errors of the Old DCHM, New DCHM1, and 4 are less 0.2 m and can be neglected when no ocean current occurs. These three methods see much smaller mean and max errors than the other three methods when under a 1 m/s ocean current, the New DCHM4 seeing the least. Ocean current can increase both mean and max errors as well.

Non-qualified distances of new DCHM1, 2, and 4 are shorter than those of other methods no matter whether there are ocean currents, the DCHM4 seeing the shortest. Non-qualified distances are independent of the length of each long section of the desired paths because they only occur near the corners of the paths.

5. Further Discussions

5.1. Why do methods using convex mapping work better?

If a convex function is used: when e is relatively large, the convex function will generate a Ψ_m that will be long lasting, thus ensuring that the large deviation will be corrected fast enough. When e is relatively small, Ψ_m changes noticeably as e changes, and the movement of the AUV can be controlled in time, thus ensuring that the small deviation will be corrected fast enough. Therefore, the convex function enables an overall faster convergence of the AUV's path following.

If a concave function is used: when e is large, Ψ_m changes rapidly, a large correction amount of Ψ_m is short lived, resulting in a very slow correction of the large deviation. When e is small, Ψ_m changes sluggishly, the AUV's heading adjustment will be slow and lagging, thus leading to a long period of convergence for the small deviation. Therefore, the concave function usually results in an overall slow convergence of the AUV's path following.

5.2. Can the proposed method be applied to non-linear paths?

The proposed method can be applied to non-linear paths, including circular and sinusoidal paths. Usually, step signal inputs such as the lawn-mower pattern paths tested in this paper, is much worse than the comparatively mild sinusoidal or circular input paths. Step input requires a higher quality or stricter response for the system to perform well. We intend to test other complex paths soon. Therefore, we can guarantee that the system will produce repeated good output responses to other mild inputs.

In addition, New DCHMs use path following error e to calculate the heading angle modification Ψ_m. The e here can be defined as the shortest distance between the AUV and any path, including linear, circular, and sinusoidal paths. New DCHMs do not exclude any complex paths.

https://doi.org/10.1017/S0263574715000867 Published online by Cambridge University Press

6. Conclusions

This paper proposes a practical guidance and control system, based on DCHM with a direct mapping function between the cross-track error e and the heading angle modification Ψ_m, used for the AUV's path following. It mainly comprises of five steps: (1) calculate the heading modification value Ψ_m using the direct mapping function between e and Ψ_m; (2) calculate the radius of the dynamic circle using Ψ_m; (3) calculate the temporary desired way point to determine the LOS vector; (4) calculate the Ψ_{LOS}; (5) control the AUV's heading to converge to the Ψ_{LOS} real time.

Several cases are tested to demonstrate the performance of the guidance and control based on the DCHMs for a real AUV. Both hydrodynamic and kinematic characteristics of the AUV are taken into account in our simulation.

The results show that methods using a convex mapping function can achieve a better convergence of path following, as well as reduce the error between the actual and desired heading angle, and the time during which such error exists. We can also customize a discretionary mapping between e and Ψ_m without intentionally selecting a mapping function between R_L and e—whose guidance performance is indistinct and is difficult to control, to get better path following performance.

Acknowledgements

This work is supported by Prospering Sea Project with Science and Technology of Tianjin (Title: Small leak detection and location system for subsea pipelines based on smart ball, No. KJXH2013-06). We thank Mr. Randy Ganye for English proofreading of this paper.

References

1. D. Ribas, N. Palomeras, P. Ridao, M. Carreras and A. Mallios, "Girona 500 AUV: From survey to intervention," *IEEE ASME Trans. Mechatron.* **17**(1), 46–53 (2012).
2. A. Bagnitsky, A. Inzartsev, A. Pavin, S. Melman and M. Morozov, "Side Scan Sonar using for Underwater Cables & Pipelines Tracking by Means of AUV," *2011 IEEE Symposium on Underwater Technology and Workshop on Scientific Use of Submarine Cables and Related Technologies* Tokyo, Japan (2011) 1–10.
3. Y. R. Petillot, S. R. Reed and J. M. Bell, "Real Time AUV Pipeline Detection and Tracking using Side Scan Sonar and Multi-Beam Echo-Sounder," *Oceans 2002 Conference and Exhibition, Conference Proceedings*, OCEANS '02 MTS/IEEE **1**, (2002) pp. 217–222.
4. D. P. Williams, "AUV-enabled adaptive underwater surveying for optimal data collection," *Intell. Serv. Rob.* **5**(1), 33–54 (2012).
5. C. Su, W. B. Yu, G. Y. Ni, Z. C. Huang, C. H. Tao and X. C. Zhang, "Display and control system for deep water multi-beam bathymetric side-scan sonar," *J. Zhejiang Univ. Eng. Sci.* **47**(6), 934–943+968 (2013).
6. Y. S. Chang, J. E. Keh, H. G. Jo and M. H. Lee, "Development of the side scan sonar using the multibeam sensors: Sensor design," *Trans. Korean Inst. Electr. Eng.* **54**(10), 581–587 (2005).
7. Q. L. Dong, Y. Z. Ouyang, Y. Y. Chen, W. H. Han and J. B. Cao, "Measuring bottom of sea target side scan sonar and multibeam sounding system," *Hydrographic Surv. Charting* **29**(5), 52–54 (2009).
8. M. Breivik and T. I. Fossen, "Principles of Guidance-Based Path Following in 2D and 3D," *Proceedings of the 44th IEEE Conference on Decision and Control and 2005 European Control Conferenc*, (2005) pp. 627–634.
9. C. Samson, "Path following and Time-Varying Feedback Stabilization of a Wheeled Mobile Robot," *Second International Conference on Automation, Robotics and Computer Vision*, Singapore **3**, (1992) pp. 1–5.
10. L. Consolini and M. Tosques, "A path following problem for a class of non-holonomic control systems with noise," *Automatica* **41**(6), 1009–1025 (2005).
11. L. Lapierre, D. Soetanto and A. Pascoal, "Nonlinear Path Following with Applications to the Control of Autonomous Underwater Vehicles," *42nd IEEE International Conference on Decision and Control*, IEEE **2**, (2003) pp. 1256–1261.
12. K. D. Do and J. Pan, "Global robust adaptive path following of underactuated ships," *Automatica* **42**(10), 1713–1722 (2006).
13. P. Encarnação and A. Pascoal, "3D Path Following for Autonomous Underwater Vehicles," *Proceedings of the 39th IEEE Conference on Decision and Control*, IEEE Snydney, NSW **3**, (2000) pp. 2977–2982.
14. M. Kothari, I. Postlethwaite and D. W. Gu, "UAV Path Following in Windy Urban Environments," *J. Intell. Robot. Syst.*, June 2014, **74**(3) pp. 1013–1028.
15. G. Q. Xia, Y. Yang and W. G. Zhao, "Path following in 3D for Underactuated AUV in the Presence of Ocean Current," *Proceedings - 2013 5th Conference on Measuring Technology and Mechatronics Automation*, IEEE, Hongkong (2013) pp. 788–791.
16. L. Lapierre and B. Jouvencel, "Robust nonlinear path-following control of an AUV," *IEEE J. Oceanic Eng.* **33**(2), 89–102 (2008).

17. D. R. Nelson, D. B. Barber, T. W. McLain and R. W. Beard, "Vector field path following for miniature air vehicles," *IEEE Trans. Robot.* **23**(3), 519–529 (2007).
18. A. Sgorbissa and R. Zaccaria, "Integrated obstacle avoidance and path following through a feedback control law," *J. Intell. Robot. Syst.*, December 2013, **72**(3) pp. 409–428.
19. L. Moreira, T. I. Fossen and S. C. Guedes, "Path following control system for a tanker ship model," *Ocean Eng.* **34**(14–15), 2074–2085 (2007).
20. W. Naeem, R. Sutton, S. M. Ahmad and R. S. Burns, "A review of guidance laws applicable to unmanned underwater vehicles," *J. Navig.* **56**(1), 15–29 (2003).
21. Y. T. Wang, W. S. Yan and W. Yan, "A Leader-Follower Formation Control Strategy for AUVs Based on Line-of-Sight Guidance," *IEEE International Conference on Mechatronics and Automation*, IEEE, Changchun (2009) pp. 4863–4867.
22. X. P. Wu, Z. P. Feng, J. M. Zhu and R. Allen, "Line of sight guidance with intelligent obstacle avoidance for autonomous underwater vehicles," *OCEANS2006* IEEE, Boston, MA (2006) 1–6.
23. X. Huang, Y. Li and S. Jin, "A Control System Based On Data Exchange Using Ethernet And CANBUS for Deep Water AUV," *9th Asian Control Conference*, Istanbul, Turkey (June 2013) 1–5.
24. M. Breivik, Nonlinear Maneuvering Control of Underactuated Ships *MSc Thesis* (Trondheim, Norway: Department of Engineering Cybernetics, Norwegian University of Science and Technology, 2003), 29–32.
25. T. I. Fossen, *Marine Control Systems: Guidance, Navigation and Control of Ships, Rigs and Underwater Vehicles*, 1st ed. (Marine Cybernetics,Trondheim, Norway 2002) pp. 105–107.

https://doi.org/10.1017/S0263574715000867 Published online by Cambridge University Press